World Electric Vehicle Journal

MDPI

Article

An Anti-Interference Control Method for an AGV-WPT System Based on UIO-SMC

Jun Hou [1,*], Weidong Huang [1] and Dongxiao Huang [2,*]

[1] School of Mechanical and Automotive Engineering, Fujian University of Technology, Fuzhou 350118, China; hwd@fjut.edu.cn

[2] National Local Joint Engineering Research Center for Electrical Drives and Power Electronics, Quanzhou Institute of Equipment Manufacturing, Haixi Institutes, Chinese Academy of Sciences, Quanzhou 362000, China

* Correspondence: a1q1s1@126.com (J.H.); dongxiao.huang@fjirsm.ac.cn (D.H.)

Abstract: During the wireless charging of an automated guided vehicle (AGV), the output voltage is unstable due to changes in parameters such as coil mutual inductance and load resistance caused by external interferences and internal mismatches of the system. In this paper, an integral sliding mode control method based on an unknown input observer (UIO) containing predictive equations is designed to build an inductor–capacitor–capacitor-series (LCC-S) topology model for wireless power transfer (WPT). The observer designed by this method can perceive changes in the secondary resistance parameter and the mutual inductance of the primary and secondary coils. The design with the prediction equation speeds up the convergence of the observer to the true value. The observer's compensation of the control system avoids the occurrence of integral oversaturation. The experimental results show that, based on the UIO-SMC system output, voltage can be accurately controlled to meet the requirement for a given voltage. The effect of suppressing disturbance is better than with SMC and PI control. When the system parameter changes, it has better voltage anti-interference performance and stronger ripple suppression.

Keywords: wireless power transfer (WPT); sliding mode control (SMC); prediction equation; unknown input observer (UIO)

Citation: Hou, J.; Huang, W.; Huang, D. An Anti-Interference Control Method for an AGV-WPT System Based on UIO-SMC. *World Electr. Veh. J.* **2021**, *12*, 220. https://doi.org/10.3390/wevj12040220

Academic Editor: Chris Mi

Received: 5 September 2021
Accepted: 29 October 2021
Published: 4 November 2021

1. Introduction

With the wide usage of automated guided vehicles (AGVs), battery life has become the main aspect affecting them, and the battery charging mode has become a hotspot for electrical engineering research. Wireless power transfer (WPT), due to its advantages of safe and reliable charging, convenient carrying, light weight, and small switch wear [1], has been studied and applied in new energy vehicles by many researchers at home and abroad, opening up a new way to improve AGV endurance.

The AGV charging system requires a reliable, efficient, and high-quality power supply. From the perspective of battery life, stability of battery charging power and diagnosis of battery charging status are required [2]. In reference [3], the author proposed to perform electrochemical impedance spectroscopy (EIS) simulation of battery impedance matching characteristics, and estimated the battery state of charge in a high-frequency WPT system. Considering the stability of battery charging power, to obtain required charging performance, the system itself needs to meet a set of performance features related to anti-interference ability, steady-state error, overshoot, and dynamic behavior, among others [4].

Various control methods have been proposed at home and abroad to improve the performance of the control system, such as adaptive control [5], robust control [6], sliding mode control [7,8], fuzzy control [9], etc. Among them, in terms of response speed and dynamic performance that meet the system requirements, sliding mode control is easy to

implement and easy to design. It is widely used in wireless power transmission system control. In the approach [7], a combination of phase shift control based on climbing search and sliding mode control theory for WPT systems with series–series topology to control the output voltage of the system was established. In the approach [8], a control method for an outer ring proportional-integral (PI) controller and inner ring sliding mode to realize constant voltage control of the WPT system was adopted.

However, in actual circuit systems, parameters such as capacitance, inductance, and resistance can change due to the influence of uncertain factors in the external environment [10]. Therefore, when designing the controller, it is necessary to consider the influence of changes in such parameters on the control effect. If disturbances are not considered when designing a sliding mode controller, non-matching errors that cannot be adjusted by robustness will occur [11,12]. Based on this situation, a composite control method based on a disturbance observer is proposed, which is more effective in solving a class of systems with non-matching disturbances. Researchers have proposed a variety of observers in the field of interference estimation, such as extended state observers (ESO), disturbance observers, generalized proportional integral observers (GPIO), and sliding mode observers (SMO) [13–17]. An ESO was proposed in [13], and an adaptive sliding mode controller based on disturbance estimation was designed to realize position tracking of the servo mechanism. The disturbance observer designed in [14] estimates the influence of the disturbance and updates the sliding manifold and control law. In another study [15], the GPIO is applied to a direct-current-direct-current (DC-DC) step-down circuit controlled by SMC to achieve a stable output voltage. In [16], the author proved that the global stability of SMC + SMO and SMO was designed to estimate load and state variables at the same time. This observer design needs to derive the system state variables, which can cause certain noise amplification problems. In [17], the author proposed a dynamic estimator for unknown systems, which is less sensitive to noise and only needs to adjust one parameter; this estimator has been widely used in actual systems.

In summary, this paper proposes an integral sliding mode control method based on unknown input observer. First, an unknown input observer is designed to observe the changes of the secondary resistance, inductance parameters, and coil coupling coefficient. A prediction function is added to the observer to ensure that the observed disturbance value quickly converges to the neighborhood of the real disturbance value. Feedforward compensation to the controller is carried out to ensure that the controller has good anti-interference ability, and to prevent the controller from generating integral oversaturation. Second, an observer is constructed that can effectively observe the mutual inductance disturbance. Speeding up the convergence speed to approach the sliding mode surface reduces chattering of the controller. Finally, a low-power wireless power transmission experiment platform is built. The effectiveness of the control method proposed in this paper is verified through experiments. To better illustrate the comparison among the proposed method in this article and other methods, the Table 1 is used to display.

Table 1. Comparison of the observer designed in this paper with those in other studies.

Observer Type	ESO[13]	SMO[16]	UIO[17]	Observer in this Paper
Number of parameters to be adjusted	3	2	1	1
Whether to add wave filter	No	No	Yes	Yes
Other features	Designed ESO can reduce control gain of SMC	Stability of SMC + SMO is proven; chattering caused by constant velocity approaching law in SMO is inevitable	Proposed and used in servo mechanism	Initial observation error is small; mutual inductance disturbance observed in WPT system, which can suppress controller chattering

When using ESO[13] and other observers of the same structure, it is necessary to consider the complexity of matching multiple parameters. Therefore, in the servo system, this type of observer is more popular. Considering that id and iq or torque and speed need to be controlled in the motor system, it is more appropriate to use an SMO[16] observer. The SMO has the feature of simultaneously observing two variables, but some noise will be introduced. In the WPT system, in order to avoid the complicated design of the observer from introducing difficulty to the system control, UIO[17] can be considered, which is simple in design and convenient to construct. In this paper, UIO is used in the WPT system, which is designed to observe mutual inductance disturbances, and reduces the initial observation error of UIO. The method proposed in this paper is suitable for use in WPT systems, where the mutual inductance changes and the output waveform is required to be stable.

2. System Topology

In a WPT system, the four basic compensation topologies, SS, SP, PS, and PP (where S represents series form and P represents parallel form), have been well researched [2]. In recent years, hybrid compensation topology has been proposed, such as inductor–capacitor–inductor-series (LCL-S) compensation topology [18]. Based on that, in order to reduce the volume of compensation inductance, LCC compensation topology is proposed with the addition of a compensation capacitor in series with the coil [19].

The primary side adopts the LCC topology structure. Constant voltage or constant current output characteristics can be realized through the topology parameter configuration and working frequency setting. These match the constant current/constant voltage charging characteristics of the battery and make it easy to realize zero voltage switching (ZVS) [20], thereby reducing switching losses. The secondary side adopts the s-type topology structure, which is beneficial to reduce the number of secondary side components and the weight of onboard equipment. Therefore, the LCC-S resonance compensation structure is selected for the system studied in this paper.

The topology of the LCC-S magnetic coupling wireless power transmission circuit system is shown in Figure 1, where E represents the DC input voltage of the system. The inverter bridge converts the DC voltage into a high-frequency alternating current, which is coupled to the secondary side through the magnetic field of the primary coil, and then converts the high-frequency alternating current into direct current through series resonance and the rectifier bridge. After the filter circuit is supplied to the battery, the equivalent load is R_L. L_p and L_s are the self-inductance of the primary and secondary coils, C_p is the compensation capacitance of the primary coil, and M is the mutual inductance value between the primary and secondary coils.

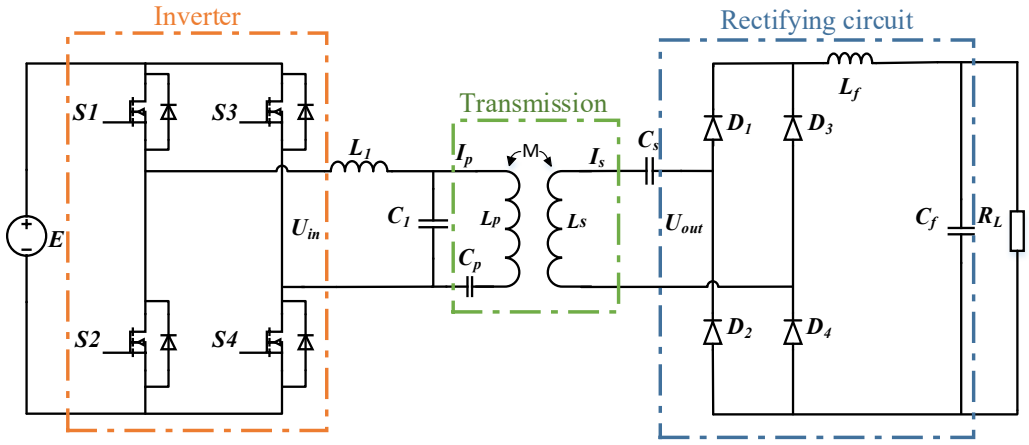

Figure 1. WPT system structure with LCC-S topology.

In order to make the primary and secondary sides of the LCC-S WPT system work in resonance and improve system efficiency, the equivalent circuit parameters shown in Figure 2 should meet the following:

$$\begin{cases} C_1 = \frac{1}{\omega^2 L_1} \\ C_s = \frac{1}{\omega^2 L_s} \\ C_p = \frac{1}{\omega^2 (L_p - L_1)} \end{cases} \tag{1}$$

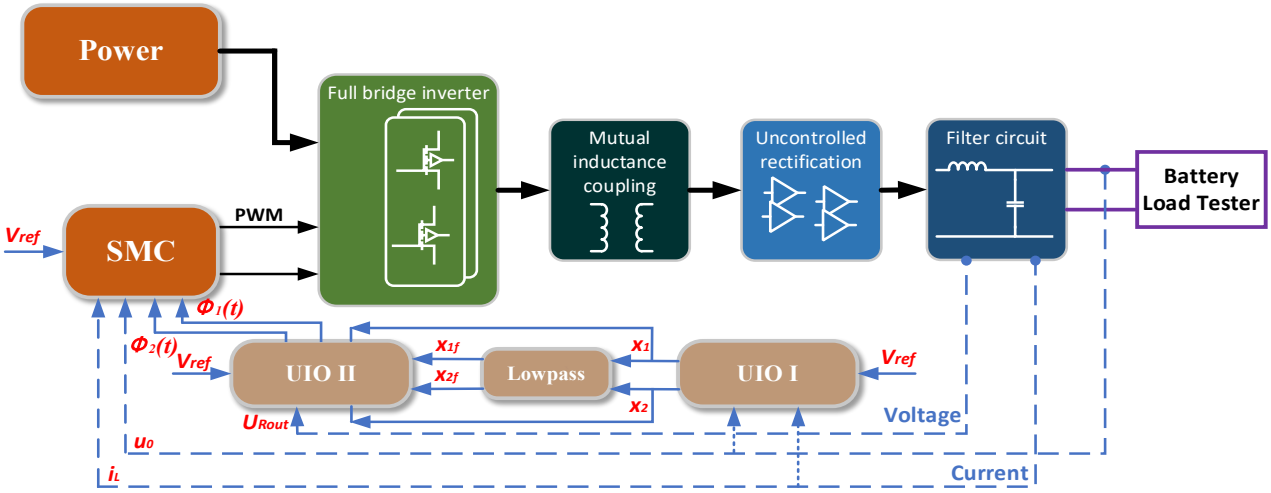

Figure 2. Block diagram of control system.

In the formula, ω is the angular frequency (rad/s) of the inverter output voltage U_{in}, and $\omega = 2\pi f$, and f is the resonant operating frequency (Hz) of the system. According to the SAEJ2954 international standard, the resonant operating frequency f of the system in this paper is set to 85 kHz.

In order to facilitate control, the system uses phase-shifted full-bridge control technology to control the output voltage of the inverter [21]. In the phase-shift power modulation mode, the duty cycle of each switch tube driving pulse is 50% and the frequency is unchanged. The duty cycle of the inverter output voltage is adjusted by adjusting the phase difference between the inverter and tube drive pulses. That is, in Figure 1, the driving pulses of S2 and S3 lag behind the driving pulses of S1 and S4 by a certain phase angle α to realize regulation of the output fundamental wave voltage.

The relationship between phase-shift angle α and fundamental effective value U_{in} of the output voltage of the high-frequency inverter is as follows:

$$U_{in} = \frac{2\sqrt{2}}{\pi} \frac{M}{L} \cos\frac{\alpha}{2} \tag{2}$$

The primary and secondary resonance in the relationship between the effective value of the inverter output voltage U_{in} and the secondary coil of current term I_P is as follows:

$$U_{in} = \omega L I_p \tag{3}$$

According to the law of electromagnetic induction, the effective value U_s of the secondary voltage is shown in Formula (4):

$$U_s = \omega M I_p \tag{4}$$

where M is the mutual inductance value between primary and secondary side coils.

The secondary circuit adopts a series resonance compensation circuit which satisfies $\omega = 1/\sqrt{C_s L_s}$. Considering the mismatch of system parameters and external interference, the effective value U_{out} of the rectifier bridge output voltage can be equivalent to Formula (5):

$$U_{out} = \omega(M + \Delta M)I_p \tag{5}$$

When the coil is offset, the mutual inductance changes by ΔM.

According to Equations (2)–(5), the relation between inverter phase-shift angle α and the effective value of U_{out} can be expressed as follows:

$$U_{out} = \frac{M + \Delta M}{L}\left(\frac{2\sqrt{2}}{\pi}E\cos\frac{\alpha}{2}\right) \tag{6}$$

3. Control System Design

3.1. Sliding Mode Controller Design

A mathematical model was established, and the tracking deviation of the load output voltage was selected as the state variable of sliding mode control. Then the tracking deviation x_1, the rate of change of tracking deviation x_2, and the integral of tracking deviation x_3 can be expressed as follows:

$$\begin{cases} x_1 = V_{ref} - u_0 \\ x_2 = \dot{x}_1 = \frac{d(V_{ref} - u_0)}{dt} = \frac{u_0}{R_L C_f} + \int \frac{u_0 - u_{eq}}{L_f C_f} dt \\ x_3 = \int x_1 dt = \int (V_{ref} - u_0) dt \end{cases} \tag{7}$$

where u_0 is the load voltage, V_{ref} is the reference voltage, and u_{eq} is a switching law control, which is equivalent to the effective value of the output voltage of the secondary side rectifier bridge.

The sliding surface is designed as follows:

$$s(x) = \alpha x_1 + x_2 + \beta x_3 \tag{8}$$

where α and β are the sliding mode coefficients and must meet the Hurwitz condition, namely, $\alpha > 0$ and $\beta > 0$.

The Lyapunov function is defined as follows:

$$V_s = \frac{1}{2}s^2 \tag{9}$$

In order to guarantee $\lim\limits_{s \to 0} s\dot{s} < 0$, the sliding mode control law is designed as follows:

$$u_{eq} = i_c L_f\left(\frac{1}{R_L C_f} - \alpha\right) + [\beta(V_{ref} - u_0) + \eta sign(s)]L_f C_f + u_0 \tag{10}$$

To solve the problem of system parameter mismatch and mutual inductance change caused by variations of the ideal charging environment, this paper proposes a control method based on UIO-SMC. Perturbation $\varphi(t)$ is introduced into the state space equation:

$$\begin{cases} \dot{x}_1 = x_2 + \varphi_1(t) \\ \dot{x}_2 = \frac{u_0 - u}{L_{f_0} C_{f_0}} + \frac{i_c}{C_{f_0}} \cdot \frac{1}{R_{L_0} C_{f_0}} + \varphi_2(t) \\ \dot{x}_3 = x_1 = V_{ref} - u_0 \end{cases} \tag{11}$$

where $\varphi_1(t)$ is the load interference quantity, $\varphi_2(t)$ is the energy transmission interference quantity. The expansions of $\varphi_1(t)$ and $\varphi_2(t)$ is shown in the following formula:

$$\begin{bmatrix} \varphi_1(t) \\ \varphi_2(t) \end{bmatrix} = \begin{bmatrix} \frac{1}{R_{L_0}C_{f_0}} - \frac{1}{R_L C_f} \\ \frac{1}{C_{f_0}}\left(\frac{1}{L_{f_0}} - \frac{1}{L_f}\right) + \frac{1}{R_{L_0}C_{f_0}} \cdot \frac{1}{R_L C_f} \end{bmatrix} u_0 + \begin{bmatrix} \frac{1}{C_f} - \frac{1}{C_{f_0}} \\ -\frac{1}{R_{L_0}C_{f_0}} \cdot \frac{1}{C_f} \end{bmatrix} i_L + \begin{bmatrix} d_1(t) \\ \frac{1}{C_{f_0}}\left(\frac{u_{eq}}{L_f} - \frac{u_{out}}{L_{f_0}}\right) + d_2(t) \end{bmatrix} \tag{12}$$

where $d_1(t)$ and $d_2(t)$ are the external interference of the system. Given $s = 0$, Formula (8) can be expressed as follows:

$$\dot{x}_1 = -\alpha x_1 - \beta \int x_1 dt + \varphi_1(t) \tag{13}$$

As can be seen, although integral sliding mode steady-state error can be compensated, it will cause slow system response and the presence of a wind-up phenomenon [22]. The estimated value is fed to the sliding surface as a feedforward compensation, as shown in Formula (14):

$$\dot{x}_1 = -\alpha x_1 - \beta \int x_1 dt + \varphi_1(t) - \hat{\varphi}_1(t) = -\alpha x_1 - \beta \int x_1 dt + d_1(t) \tag{14}$$

Employing compensation, the system hysteresis caused by the integral term is reduced, integral supersaturation is reduced, and the reaction speed of the system is improved.

As shown in Equations (3) and (5) above, the system will inevitably encounter disturbance in the energy transmitting terminal and energy transmission. It can be seen from Equation (6) that the disturbance will be reflected in the energy receiving terminal. We can observe the disturbance value at the energy receiving terminal and provide compensation for the system.

3.2. Unknown Input Observer Design

In the wireless power transmission system, changes in parameters such as capacitance, inductance, and resistance at operating temperature, or other reasons, will cause the parameter values to change. The parameter change value can be regarded as a kind of disturbance to the control system: if left alone, it will affect the control performance. Conversely, for the primary and secondary coils that transmit energy, any change in their relative position will affect the mutual inductance of the system. Formula (6) derivation shows that a change of mutual inductance will directly affect the output voltage of the system. Therefore, it is necessary to design a feedback control to address the influence of disturbance caused by parameter changes in the system. This paper proposes an unknown input observer to estimate disturbances in the secondary side parameters of the system and the mutual inductance between the coils. Feedforward compensation to the sliding mode controller is used to eliminate the influence of integral saturation on the control system.

In the design of the unknown input observer, the variable filter is defined, as shown in Formula (15):

$$\begin{bmatrix} x_1 \\ x_2 \end{bmatrix} = \lambda \begin{bmatrix} \dot{x}_{1f} \\ \dot{x}_{2f} \end{bmatrix} + \begin{bmatrix} x_{1f} \\ x_{2f} \end{bmatrix} \quad \begin{cases} x_{1f}(0) = 0 \\ x_{2f}(0) = 0 \end{cases} \tag{15}$$

where λ is the filtering time constant, and $\lambda > 0$.

At the initial time, the value of the filtering variable x_{1f} is 0, and the initial value of x_1 is $Vref$.

After the observation value is magnified, the observer has a larger error at the initial moment. It is easy to produce overshoot during feedforward compensation of the control system. When the control system includes an integral function, it is easy to produce

oversaturation. The same thing applies to x_{2f}. For the dynamic performance of the system, the following unknown input observers are designed:

$$\begin{bmatrix} \hat{\varphi}_1(t) \\ \hat{\varphi}_2(t) \end{bmatrix} = \begin{bmatrix} -\frac{1}{\lambda} & -1 \\ \frac{1}{C_{f_0} L_{f_0}} & -\frac{1}{\lambda} \end{bmatrix} \begin{bmatrix} x_{1f} \\ x_{2f} \end{bmatrix} + \begin{bmatrix} \frac{x_1}{\lambda} - \sigma^k x_1 \\ \frac{x_2}{\lambda} - \frac{U_{out}}{C_{f_0} L_{f_0}} + \frac{V_{ref}}{C_{f_0} L_{f_0}} - \sigma^k x_2 \end{bmatrix} \tag{16}$$

Formula (16) satisfies $\lim\limits_{\substack{\lambda \to 0 \\ t \to \infty}} \hat{\varphi}_1(t) = 0$ and $\lim\limits_{\substack{\lambda \to 0 \\ t \to \infty}} \hat{\varphi}_2(t) = 0$.

In the formula, $\sigma^k x$ is the prediction equation, which means that the prediction of changes x_1 uses the exponential function to converge. $0 < \sigma < 1$, according to the system, selects $\sigma = 0.99$, $k = T/Ts$, where k is the current time divided by the control period. The selection of filter time constant λ was analyzed in [23], and $\lambda = 0.001$ was selected here for better tracking.

The filter variables φ_{1f} and φ_{2f} are defined, and the relationship with the disturbance variables $\varphi_1(t)$ and $\varphi_2(t)$ is as follows:

$$\begin{bmatrix} \varphi_1(t) \\ \varphi_2(t) \end{bmatrix} = \lambda \begin{bmatrix} \dot{\varphi}_{1_f} \\ \dot{\varphi}_{2_f} \end{bmatrix} = \begin{bmatrix} \varphi_{1_f} \\ \varphi_{2_f} \end{bmatrix} \tag{17}$$

Defining errors $s_1 = \varphi_1(t) - \hat{\varphi}_1(t)$ and $s_2 = \varphi_2(t) - \hat{\varphi}_2(t)$, taking the derivative of error variables s_1 and s_2, and substituting Equation (16) into the formula, we obtain the following:

$$\begin{bmatrix} \dot{s}_1 \\ \dot{s}_2 \end{bmatrix} = -\frac{1}{\lambda} \begin{bmatrix} s_1 \\ s_2 \end{bmatrix} + \begin{bmatrix} \dot{\varphi}_1(t) \\ \dot{\varphi}_2(t) \end{bmatrix} \tag{18}$$

It is assumed that disturbances $\varphi_1(t)$ and $\varphi_2(t)$ are bounded and have $\sup_{t \geq 0} |\dot{\varphi}_1(t)| \leq \varphi_1{}^*(t)$ and $\sup_{t \geq 0} |\dot{\varphi}_2(t)| \leq \varphi_2{}^*(t)$, where sup represents the supremum of the parameter. Taking the Lyapunov function as $V_s = \frac{1}{2} s_1^2 + \frac{1}{2} s_2^2$, and taking the derivative of it, we obtain the following:

$$\begin{aligned} \dot{V}_s &= s_1 \dot{s}_1 + s_2 \dot{s}_2 \\ &\leq -\tfrac{1}{2k} s_1^2 + \tfrac{k}{2} \varphi_1^{*2}(t) - \tfrac{1}{2k} s_2^2 + \tfrac{k}{2} \varphi_2^{*2}(t) \end{aligned} \tag{19}$$

According to the differential equation, s_1 and s_2 are bounded, and Equation (20) can be obtained as follows:

$$\begin{cases} |s_1| = \sqrt{s_1^2} \leq \sqrt{s_1^2(0) e^{-\frac{t}{\lambda}} + \lambda^2 \varphi_1^{*2}(t)} \\ |s_2| = \sqrt{s_2^2} \leq \sqrt{s_2^2(0) e^{-\frac{t}{\lambda}} + \lambda^2 \varphi_2^{*2}(t)} \end{cases} \tag{20}$$

It can be inferred that when $\lambda \to 0$ and $t \to \infty$, we have $s_1 \to 0$ and $s_2 \to 0$. The system converges to the equilibrium point in a finite time. Replacing the disturbance term in Formula (11) with the observed value, the equivalent control law of the integral sliding mode controller based on the unknown input observer (UIO-SMC) is as follows:

$$u = i_c L_f \left(\frac{1}{R_L C_f} - \alpha \right) + [\alpha \hat{\varphi}_1(t) + \hat{\varphi}_2(t) + \beta x_1 + \eta sign(s)] L_f C_f + u_0 \tag{21}$$

The equivalent control expression, u, contains the system parameters R_L and C_f. In order to reduce the interference of system parameter deviation and load change on the control function, when selecting system control parameters, they should meet the following condition:

$$\alpha >> \frac{1}{R_L C_f} \tag{22}$$

4. Verification and Discussion

4.1. System Structure Design

In order to verify the anti-jamming performance of the integral sliding mode control method based on the unknown input observer in the WPT system and the estimation accuracy of the unknown input observer to the disturbance, a system structure was designed, as shown in Figure 2. MATLAB/Simulink was used to establish the system model and design simulations and experiments. In the actual system, changes in the inductance and capacitance parameters at the receiving end are not obvious, but a change in the resistance parameter will have a great influence on the output voltage. The deviation of the distance between coils in the energy transmission will affect the system; it will cause the mutual inductance to change and make the output voltage of the receiving end unstable. Therefore, we designed a simulation experiment of load resistance and coil mutual inductance changes.

The model parameters are shown in Table 2, the control parameters are shown in Table 3, and the simulation results are shown in Figures 3–5.

Table 2. Model parameters of WPT system.

Description/Unit	Parameter	Value
Inverter input DC voltage (V)	E	18
Inverter frequency (kHz)	*f*	85
Primary side topological inductance (μH)	*L1*	31
Primary side coil inductance (μH)	*Lp*	79
Primary sideline compensation capacitor (nF)	*Cp*	33
Primary topology resonance capacitance (nF)	*C1*	47
Secondary side coil inductance (μH)	*Ls*	70
secondary side resonant capacitance (nF)	*Cs*	56
Filter inductance (μH)	*Lf*	100
Filter capacitor (μF)	*Cf*	470

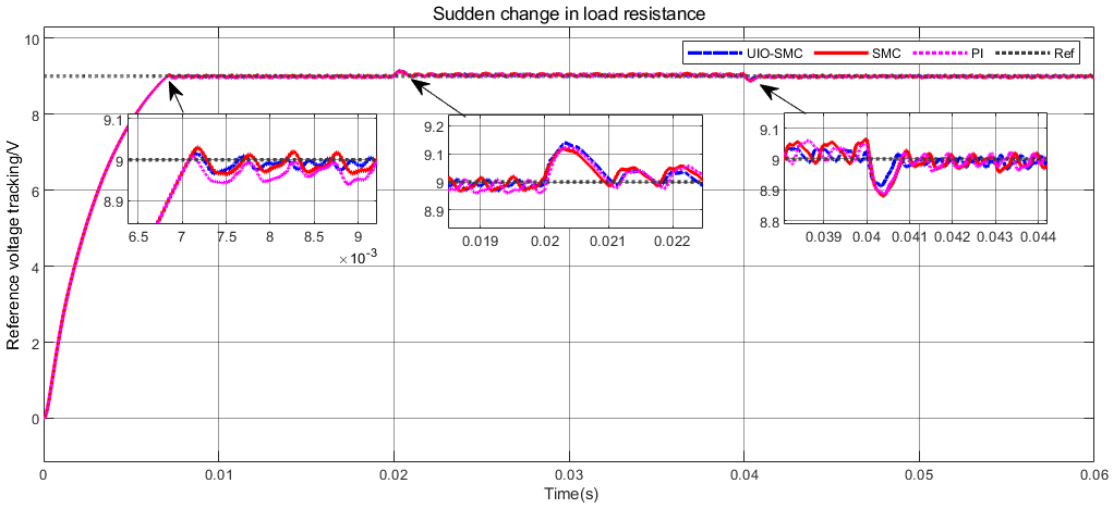

(**a**)

Figure 3. *Cont.*

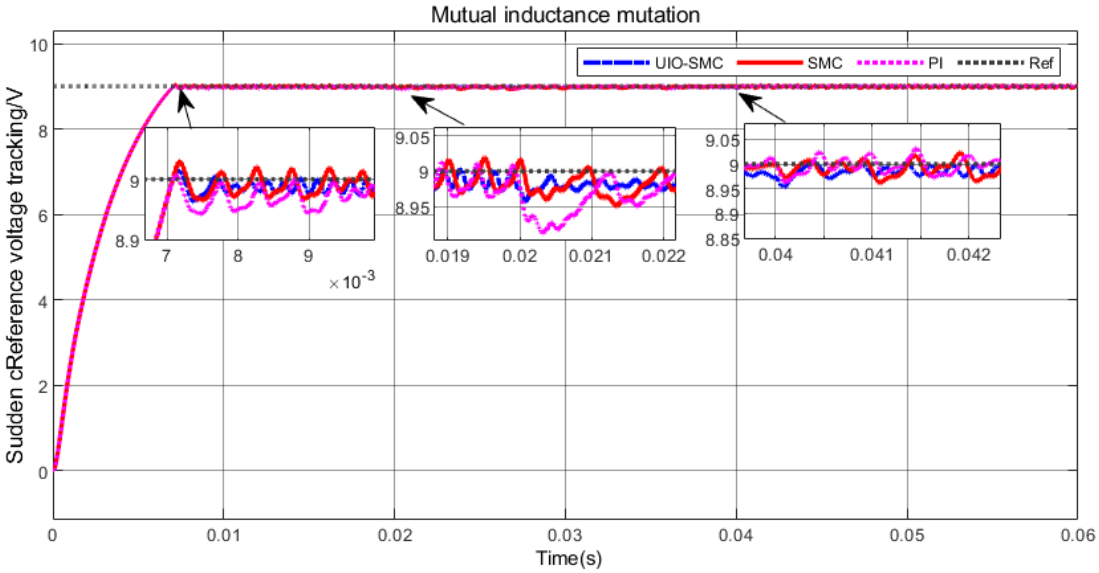

(**b**)

Figure 3. Reference voltage tracking: (**a**) sudden change of load resistance: 5 Ω → 20 Ω → 5 Ω; (**b**) mutual inductance change: 17 μH → 32 μH → 17 μH.

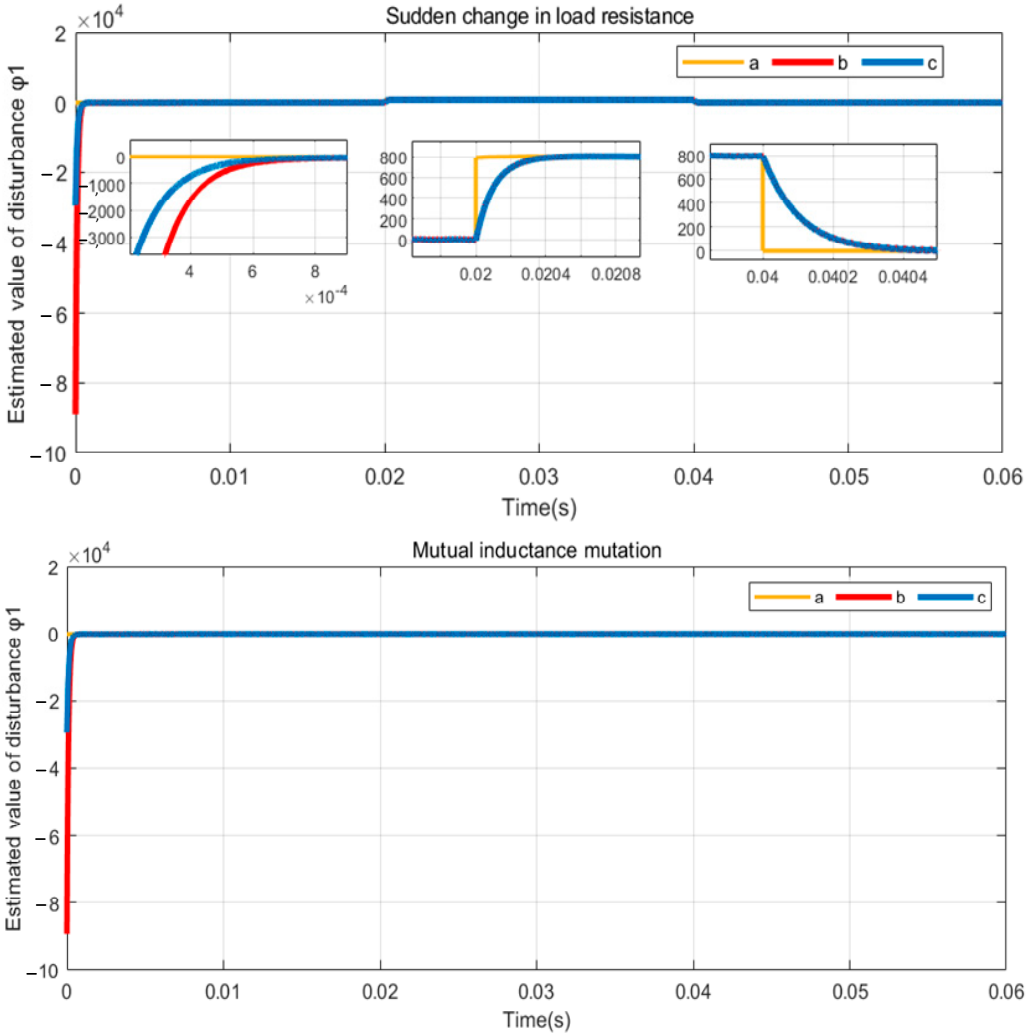

(**a**)

Figure 4. *Cont.*

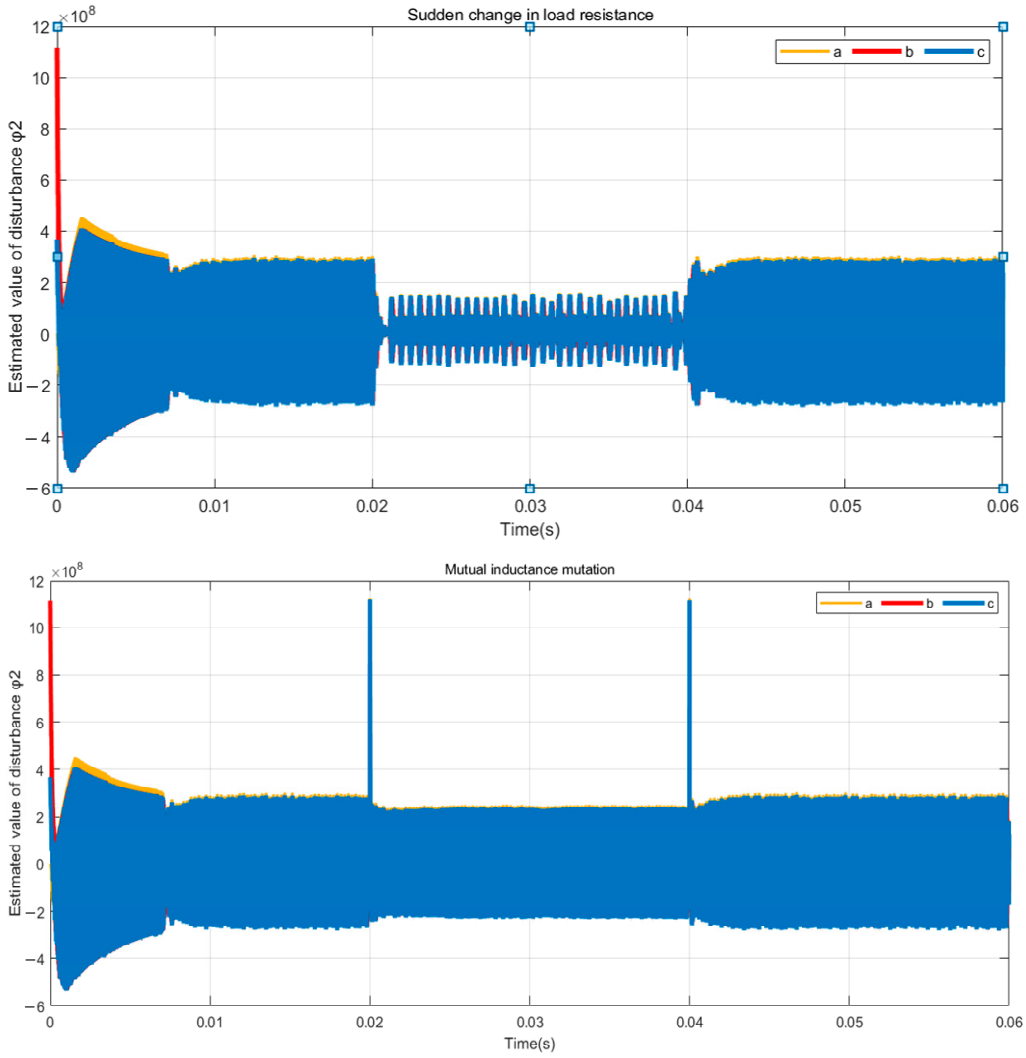

(**b**)

Figure 4. Disturbance and value estimated by observer: (**a**) estimated value of disturbance φ1; (**b**) estimated value of disturbance φ2. In the graphs, a indicates estimated amount of disturbance, b indicates UIO without adding prediction equation, and c indicates UIO added to prediction equation.

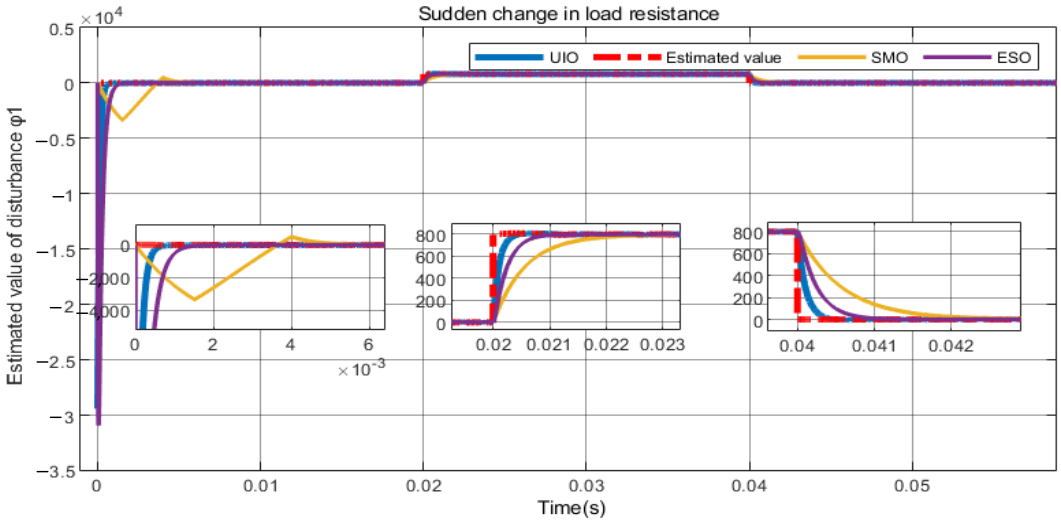

Figure 5. Estimated value of disturbance $\varphi_1(t)$ under different observers.

Table 3. Control parameters.

Control Parameter	Value
λ	0.001
σ	0.99
α	6.6×10^6
β	3×10^{13}
η	1
kp	1.2
ki	180

Choosing an appropriate sliding mode coefficient will ensure good dynamic performance of the output voltage. The selection of sliding mode coefficient must satisfy the existence condition of sliding mode. Substituting $S = 0$ into Equation (8), we obtain the following:

$$\alpha x_1 + x_2 + \beta x_3 = 0 \tag{23}$$

Substituting Formula (7) into Formula (23) for further transformation, we obtain the following:

$$\alpha x_1 + \frac{dx_1}{dt} + \beta \int x_1 dt = 0 \tag{24}$$

Equation (24) is derived from the time to obtain the standard second-order system equation as follows:

$$\ddot{x}_1 + 2\zeta\omega_n \dot{x}_1 + {\omega_n}^2 x_1 = 0 \tag{25}$$

In the formula, ζ is the damping coefficient, $\zeta = \frac{1}{2}\alpha$, and ω_n is the undamped natural oscillation frequency, $\omega_n = \sqrt{\beta}$.

The second-order system mainly has three types of responses: under-damped ($0 < \zeta < 1$), critically damped ($\zeta = 1$), and over-damped ($\zeta > 1$). In this paper, integral sliding mode control based on the law of constant velocity is adopted, and the design requires a fast approach to the sliding mode surface. Therefore, we designed the sliding mode coefficient for the over-damped state [24]. The attenuation coefficient $\tau = 1/(\zeta\omega_n)$ and damping coefficient ζ represent the adjustment time and oscillation of the system, respectively. From the calculation formula of attenuation coefficient τ and damping coefficient ζ, the relationship between sliding mode coefficients α and β can be expressed as follows:

$$\begin{cases} \alpha = \frac{2}{\tau} \\ \beta = \frac{1}{\tau^2\zeta^2} \end{cases} \tag{26}$$

In [24], the author analyzed the relationship between damping ratio, overshoot, and response time, and generally selected ζ = 0.4–0.8; this paper selects ζ = 0.6. The attenuation coefficient τ represents the dynamic response of the controller, which is mainly determined by the system power level and switching frequency [25]. If τ is too large, the system response time will be longer. If τ is too small, the system response becomes faster, but the performance requirements of the system controller are too high, and system stability is reduced. At the same time, the selection of τ must satisfy the sliding mode existence condition (10) and the assumption condition (22). Here, the parameters were selected based on the restriction conditions of the parameter selection described above. Considering that the sliding mode control law contains L_f and C_f, and the parameters of L_f and C_f are smaller, for the dynamic response performance and stability of the system, the control parameters need to be enlarged by corresponding multiples. Based on these considerations, the sliding mode control parameters are selected as follows:

$$\alpha = 6.6 \times 10^6,\ \beta = 3 \times 10^{13}.$$

The parameters of the PI controller are designed based on the rated system parameters. Because the system parameters and reference values change under different working conditions, it is difficult for the designed PI controller to achieve the same optimization under different working conditions. However, it can be seen from the actual test results that the PI parameters were optimally designed to imitate an actual application; thus, they can be compared with the effect of the sliding mode controller.

The values of the system parameters are shown in Table 3.

4.2. Analysis of Simulation Result

4.2.1. Controller Performance

The reference voltage was set to 9 V. In order to verify the output voltage anti-offset ability of the UIO-SMC under mutual inductance changes and load mutations, an output voltage comparison experiment of PI control and SMC control was designed. The output voltage waveform of the system under sudden load changes is shown in Figure 3. As shown in Figure 3a, the load changes from 5 to 20 to 5 Ω, and the changing moments are at 0.02 and 0.04 s. As shown in Figure 3b, the mutual inductance changes from 17 to 32 to 17 μH, which corresponds to the change in vertical distance of the coil from 7 to 4 to 7 cm, and the time of change is 0.02 s and 0.04 s. It can be seen from the figure that the output voltage of the three control strategies can be stabilized at the reference voltage value, but the ripple size has a more obvious difference. The output voltage ripple based on UIO-SMC control is 80% less than that of PI control and SMC control.

When the load resistance changes, since $\varphi_1(t)$ and $\varphi_2(t)$ are parameters that include loads, the observer can observe their numerical changes. When the mutual inductance changes, according to Formula (5), the input voltage at the receiving end changes within the observation range of $\varphi_2(t)$; thus, $\varphi_1(t)$ does not change at this time, and $\varphi_2(t)$ changes. It can be seen from Figure 4 that the observer proposed in this paper greatly reduces the initial error and shortens the time to converge to the true value.

The above simulation results show that the sliding mode controller based on the unknown input observer in the WPT system has strong anti-interference ability. The disturbance observer can accurately observe the disturbance and perform feedforward compensation for the sliding mode controller.

4.2.2. Observer Performance

In order to compare the UIO proposed in this paper, ESO[13] and SMO[16] are used in this section to observe disturbance $\varphi_1(t)$. The experimental results are shown in Figure 5. It can be found that the proposed UIO has better observation performance than ESO and SMO. Comparing the performance of UIO and ESO, it can be seen that although ESO can observe system disturbances, compared with UIO, it has a larger initial observation error.

4.3. Analysis of Experimental Results

In order to verify the control method proposed in this paper, an experimental platform based on TMS320F28027DSP as the control core was built. The experimental setup is shown in Figure 6. In the load mutation experiment, the distance between the transmission coils was 7 cm. In the coil offset experiment, the load resistance was 5 Ω.

4.3.1. Coil Offset Experiments

The reference voltage was set to 9 V. In this paper, a coil offset experiment was designed to correspond to the change of mutual inductance in the simulation.

Figure 7 shows the changes in the mutual inductance of the coil under different vertical distances. The mutual inductance value of the coil in the picture was measured by the LCR method in an open loop [26]. Figure 8 shows the waveform of load output voltage u_0, load output current i_0, and secondary rectifier current i_s when the coil changes from a vertical distance of 7 to 4 cm and then back to 7 cm.

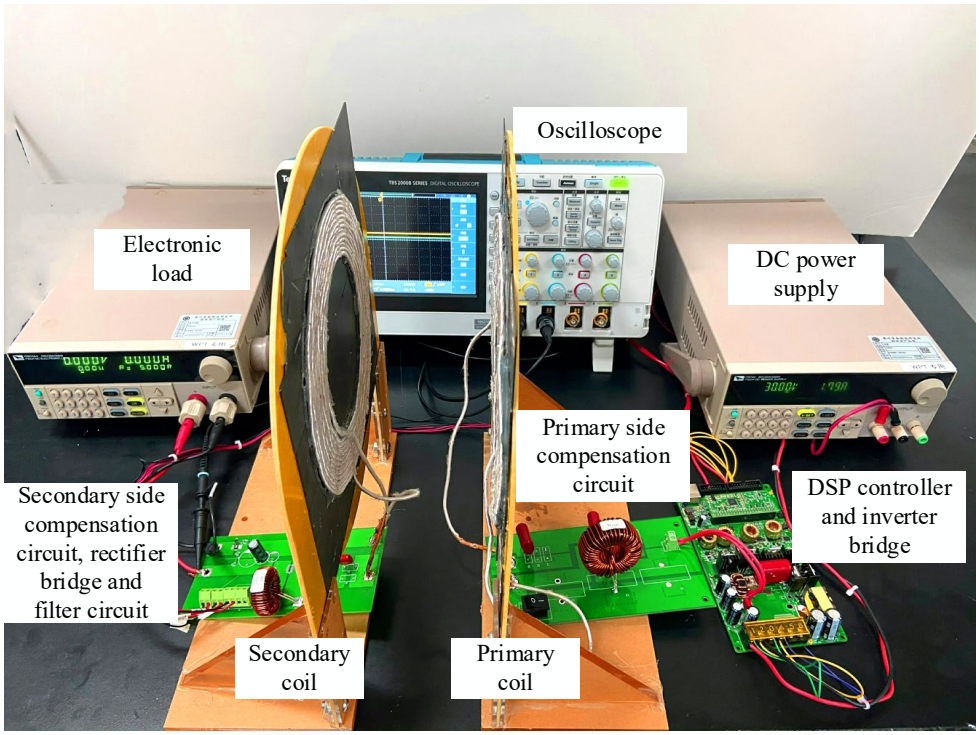

Figure 6. Exterior appearance of experimental setup.

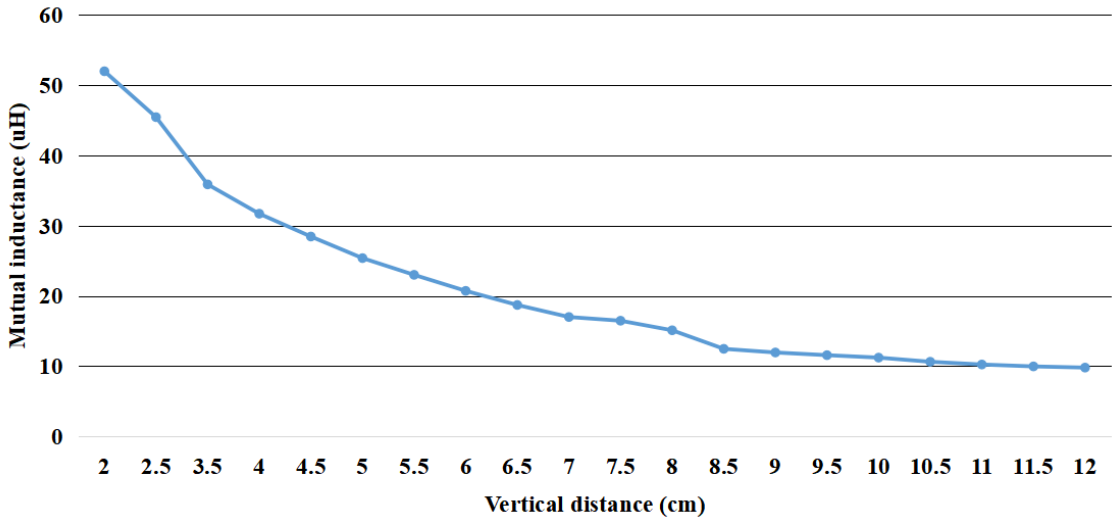

Figure 7. Relationship between vertical distance of coil and mutual inductance.

Figure 8a shows that the output voltage ripple of the sliding mode control added to the observer is smaller. This indicates that the chattering of the controller is suppressed.

4.3.2. Load Mutation Experiments

The experimental design load resistance changed from 5 to 20 to 5 Ω, and the experimental waveforms are shown in Figure 6. The response time of the control method proposed in this paper was 0.4 and 0.8 ms, the response time of the sliding mode control was 1 and 1.2 ms, and the response time of PI was 1.2 and 1.4 ms. Compared with the control method proposed in this paper, the response times of sliding mode and PI control were longer. It can be seen from Figure 9a that when the load changed to 5 Ω, the output voltage ripple of the proposed control method was smaller than that of SMC and PI control.

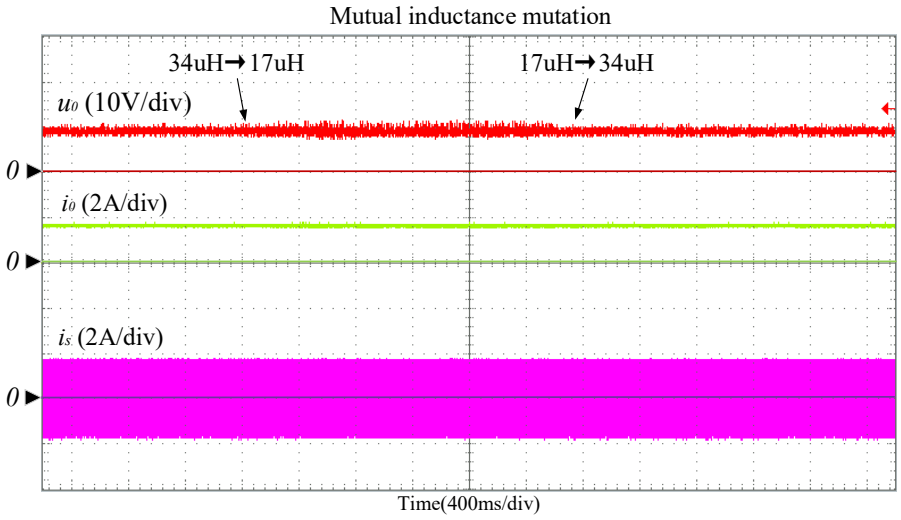

(**a**)

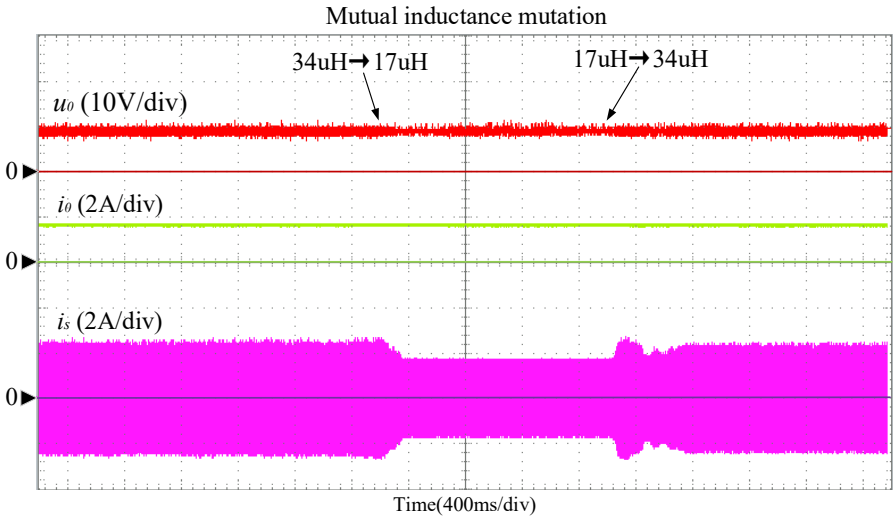

(**b**)

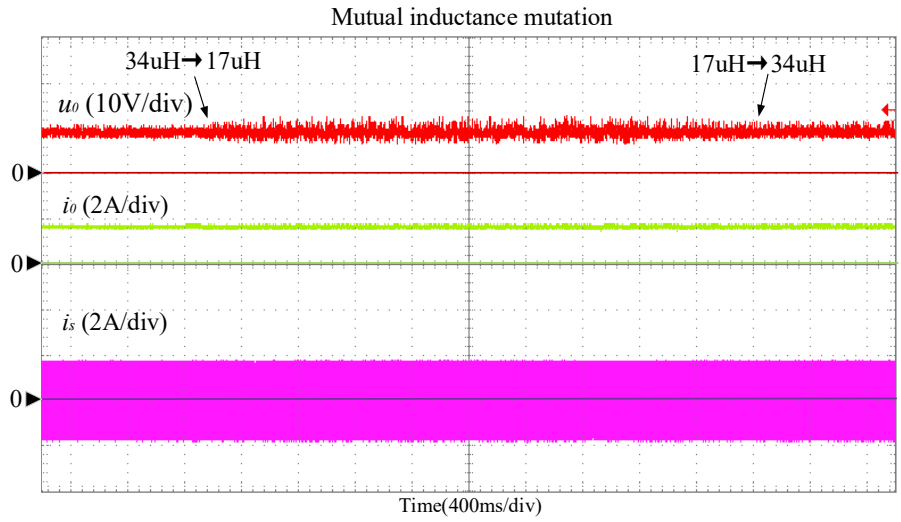

(**c**)

Figure 8. Output waveforms under change of mutual inductance: (**a**) UIO-SMC; (**b**) SMC; (**c**) PI.

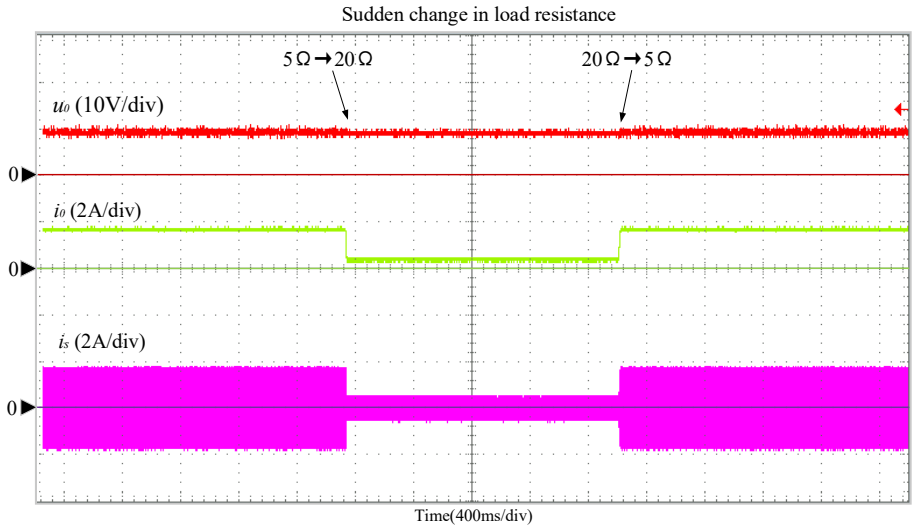

(**a**)

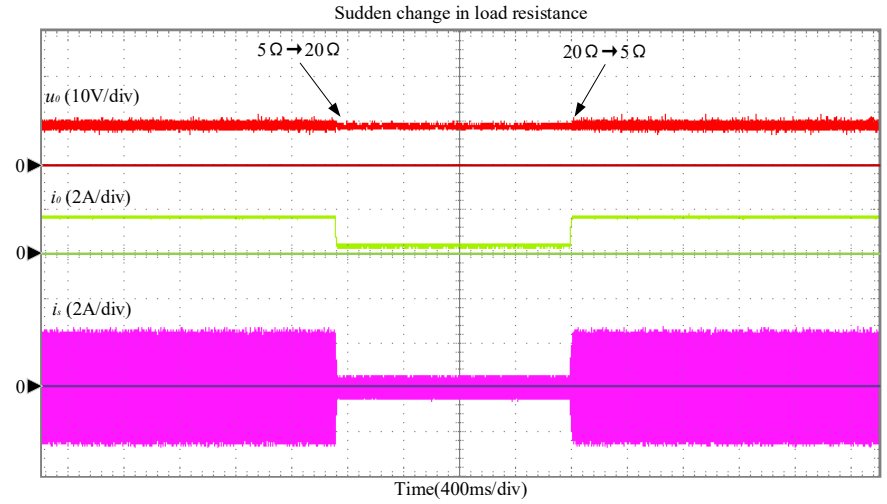

(**b**)

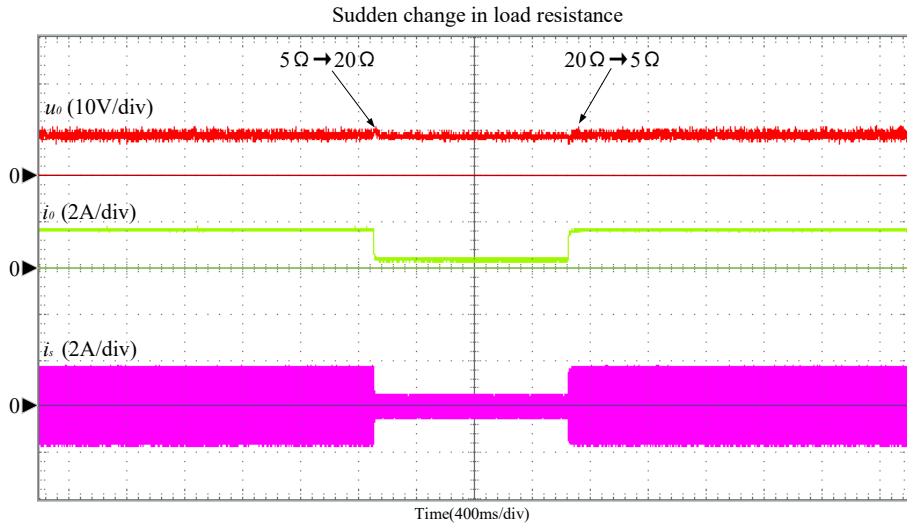

(**c**)

Figure 9. Output waveforms under sudden change in resistance: (**a**) UIO-SMC; (**b**) SMC; (**c**) PI.

5. Conclusions

This paper proposes an integral sliding mode control method based on an unknown input observer. The unknown output observer is designed based on the first-order low-pass filter. The method achieves estimation and feedforward compensation of the secondary side resistance parameters and coil mutual inductance mismatch to give the system better anti-interference ability. At the same time, a prediction equation is added to the design of the unknown input observer. The initial observation error of the observer becomes smaller, and the time to converge to the true value becomes shorter. The observer is combined with an integral sliding mode controller. While integral saturation is effectively suppressed, the robustness of the controller is improved and the chattering of the controller is reduced. The designed observer proves that the error between the observed and true values can converge to zero. The stability of the observer is proven by Lyapunov's theorem, and a brief comparison with ESO[13] and SMO[16] is made. The experimental results show that the robustness and dynamic performance of the proposed control method in WPT systems are better than those of traditional PI and sliding mode control. This method can be used to solve the disturbance problem caused by coil offset and load change during wireless charging of AGVs. In this paper, an uncontrolled rectifier bridge is selected at the rectifier side. In order to better integrate battery BMS management in the future, it can be changed as a semi-controlled or controllable full bridge to realize the regulation of power and efficiency under the condition of original anti-disturbance stable voltage output.

Author Contributions: Conceptualization, J.H.; methodology, J.H.; software, J.H.; validation, J.H.; formal analysis, J.H.; investigation, J.H.; resources, D.H. and W.H.; data curation, J.H.; writing—original draft preparation, J.H.; writing—review and editing, D.H.; visualization, D.H.; supervision, J.H. and D.H.; project administration, J.H.; funding acquisition, W.H. All authors have read and agreed to the published version of the manuscript.

Funding: This research was funded by STS Plan in Fujian Province under Grant No. 2020T3016.

Institutional Review Board Statement: Not applicable.

Informed Consent Statement: Not applicable.

Data Availability Statement: Data sharing not applicable.

Conflicts of Interest: The authors declare no conflict of interest.

References

1. Patil, D.; Mcdonough, M.K.; Miller, J.M.; Fahimi, B.; Balsara, P.T. Wireless Power Transfer for Vehicular Applications: Overview and Challenges. *IEEE Trans. Transp. Electrif.* **2018**, *4*, 3–37. [CrossRef]
2. Watrin, N.; Blunier, B.; Miraoui, A. Review of adaptive systems for lithium batteries State-of-Charge and State-of-Health estimation. In Proceedings of the 2012 IEEE Transportation Electrification Conference and Expo (ITEC), Dearborn, MI, USA, 18–20 June 2012; pp. 1–6.
3. Locorotondo, E.; Corti, F.; Pugi, L.; Berzi, L.; Reatti, A.; Lutzemberger, G. Design of a Wireless Charging System for Online Battery Spectroscopy. *Energies* **2021**, *14*, 218. [CrossRef]
4. Corti, F.; Reatti, A.; Nepote, A.; Pugi, L.; Pierini, M.; Paolucci, L.; Grasso, F.; Grasso, E.; Nienhause, M. A Secondary-Side Controlled Electric Vehicle Wireless Charger. *Energies* **2020**, *13*, 6527. [CrossRef]
5. Shi, L.; Alou, P.; Oliver, J.; Rodriguez, J.C.; Delgado, A.; Cobos, J.A. A self-adaptive wireless power transfer system to cancel the reactance. *IEEE Trans. Ind. Electron.* **2020**, *28*, 3044817. [CrossRef]
6. Naghash, R.; Alavi, S.M.M.; Afjei, S.E. Robust Control of Wireless Power Transfer Despite Load and Data Communications Uncertainties. *IEEE Trans. Emerg. Sel. Top. Power Electron.* **2020**, *9*, 4897–4905. [CrossRef]
7. Yang, Y.; Zhong, W.; Kiratipongvoot, S.; Tan, S.; Hui, S.Y.R. Dynamic Improvement of Series–Series Compensated Wireless Power Transfer Systems Using Discrete Sliding Mode Control. *IEEE Trans. Power Electron.* **2018**, *33*, 6351–6360. [CrossRef]
8. Smagulova, A.; Lu, M.; Darabi, A.; Bagheri, M. Simulation Analysis of PI and Fuzzy Controller for Dynamic Wireless Charging of Electric Vehicle. In Proceedings of the 2020 IEEE International Conference on Environment and Electrical Engineering and 2020 IEEE Industrial and Commercial Power Systems Europe (EEEIC/I&CPS Europe), Madrid, Spain, 9–12 June 2020; pp. 1–6. [CrossRef]
9. Yuan, L.; Wang, J.; Chen, G.; Zhang, Z.; Tang, C. Tracking method of optimal efficiency point of wpt system based on fuzzy control. *Guangdong Electr. Power* **2018**, *31*, 52–58.

10. Sohn, Y.H.; Choi, B.H.; Lee, E.S.; Lim, G.C.; Cho, G.H.; Rim, C.T. General Unified Analyses of Two-Capacitor Inductive Power Transfer Systems: Equivalence of Current-Source SS and SP Compensations. *IEEE T. Transp. Electr.* **2015**, *30*, 6030–6045. [CrossRef]
11. Li, S.; Yang, J.; Wu, B.; Li, Q.; Wang, J. Finite-time disturbance observer based non-singular terminal sliding mode control for pulse width modulation based DC-DC buck converters with mismatched load disturbances. *IET Power Electron.* **2016**, *9*, 1995–2002.
12. Zheng, C.M.; Zhang, J.S.; Chen, R. Discrete-time sliding mode control based on improved disturbance compensation reaching law. *Control. Decis.* **2019**, *34*, 880–884.
13. Wang, S.; Yu, H.; Gao, X.; Liu, X. ESO-Based Adaptive Sliding Control for Nonlinear Servo System with Unknown Disturbance and Uncertainties. In Proceedings of the 2018 10th International Conference on Modelling, Identification and Control (ICMIC), Guiyang, China, 2–4 July 2018; pp. 1–5.
14. Maqsood, H.; Qu, Y. Nonlinear Disturbance Observer Based Sliding Mode Control of Quadrotor Helicopter. *J. Electr. Eng. Technol.* **2020**, *15*, 1453–1461. [CrossRef]
15. Rong, J.; Yang, H.; Wang, J.; Yu, L. Design and implementation of GPI observer based sliding mode control for DC-DC buck converter. In Proceedings of the 2019 Chinese Automation Congress (CAC), Hangzhou, China, 22–24 November 2019; pp. 4256–4261. [CrossRef]
16. Jaafar, A.; Godoy, E.; Lefranc, P.; Shi, X.L.; Fayaz, A.; Nan, L. Nonlinear Sliding Mode Observer and Control of High Order DC-DC Converters. In Proceedings of the IECON 2010—36th Annual Conference on IEEE Industrial Electronics Society, Glendale, AZ, USA, 7–10 November 2010; pp. 180–186. [CrossRef]
17. Wang, S.; Na, J.; Ren, X.; Yu, H.; Yu, J. Unknown input observer-based robust adaptive funnel motion control for nonlinear servomechanisms. *Int. J. Robust Nonlinear Control.* **2018**, *18*, 6163–6179. [CrossRef]
18. Chwei-Sen, W.; Covic, G.A.; Stielau, O.H. Investigating an LCL load resonant inverter for inductive power transfer applications. *IEEE Trans. Transp. Electrif.* **2004**, *19*, 995–1002.
19. Pantic, Z.; Bai, S.; Lukic, S.M. ZCS LCC-Compensated resonant inverter for inductive-power-transfer application. *IEEE Trans. Ind. Electron.* **2011**, *58*, 3500–3510. [CrossRef]
20. Corti, F.; Paolucci, L.; Reatti, A.; Grasso, F.; Pugi, L.; Tesi, N.; Grasso, E.; Nienhaus, M. A Comprehensive Comparison of Resonant Topologies for Magnetic Wireless Power Transfer. In Proceedings of the 2020 IEEE 20th Mediterranean Electrotechnical Conference (MELECON), Palermo, Italy, 16–18 June 2020; pp. 582–587. [CrossRef]
21. Cai, H.; Shi, L.; Li, Y. Output Power Adjustment in Inductively Coupled Power Transfer System. *Trans. China Electrotec. Soc.* **2014**, *29*, 215–220.
22. Tarbouriech, S.; Turner, M. Anti-windup design: An overview of some recent advances and open problems. *IET Control. Theory Appl.* **2009**, *3*, 1−19. [CrossRef]
23. Na, J.; Chen, A.S.; Herrmann, G. Vehicle Engine Torque Estimation via Unknown Input Observer and Adaptive Parameter Estimation. *IEEE Trans. Veh. Technol.* **2018**, *67*, 409–422. [CrossRef]
24. Zhong, B.; Tang, L. Design and Simulation on PID Variable Damping Ratio Controller of Second-Order System. In Proceedings of the 2010 2nd International Conference on Information Engineering and Computer Science, Wuhan, China, 25–26 December 2010; pp. 1–4. [CrossRef]
25. Liu, J.; Xiao, F.; Ma, W.; Fan, X.; Chen, W. PWM-Based sliding mode controller for three-levelfull-bridge DC-DC converter that eliminates static output voltage error. *J. Power Electron.* **2015**, *15*, 378–388. [CrossRef]
26. Zhou, S. Design and study on a precision LCR measurement system. *J. Electron. Meas. Instrum.* **2003**, *3*, 1–5.